electronics

MDPI

Article

Research and Discussion on Thermal Model Equivalent Methods of the Random Winding

Zutao Chen, Zhongjun Yu *, Juntan Yang and Jia Fu

National Key Laboratory of Electromagnetic Energy, Naval University of Engineering, Wuhan 430033, China; zutaochen@buaa.edu.cn (Z.C.); d202380555@hust.edu.cn (J.Y.); d22180813@nue.edu.cn (J.F.)
* Correspondence: d22180815@nue.edu.cn

Abstract

Accurate thermal modeling of windings is critical for predicting motor temperature distributions when using the computational fluid dynamics (CFD) method. To solve this problem, the concentrated and anisotropic equivalent methods of random winding was systematically analyzed, and a layered equivalent strategy that simplifies the random winding into a multilayer concentric structure of copper and insulation was proposed. Then, a single-tooth random winding model was established by full model, concentrated, layered and anisotropic equivalent methods, and the steady-state and transient temperature field were carried out. The temperature experiment of single-tooth winding samples shows that all models show high accuracy in temperature calculation, exhibiting a maximum relative error below 2.9%. Furthermore, a comprehensive comparison of modeling dimensions, meshing, computational time, and result accuracy was conducted, summarizing the advantages and limitations of each method. The results indicate that the efficiency of the three equivalent methods is significantly improved compared with the full model. The maximum mesh elements shall not exceed 16% of the full model, with computational time reduced by over 75%. The results of this paper also clarify the applicable boundaries of various methods, providing a basis for the selection of motor thermal design.

Keywords: equivalent thermal model; random winding; temperature field; layered equivalent

1. Introduction

With the rapid advancement of electrification in different fields of society, the demand for high power-density and high-efficiency motors is increasing, and the rapid and accurate evaluation of various motor states has become an inevitable demand. As one of the key components of the motor, the efficient calculation of the temperature characteristics of the winding is of great significance, which is an important basis for the effective design and safe operation of the motor. Therefore, studying rapid and accurate calculation methods for the temperature field of motor winding and perceiving the temperature distribution characteristics inside the winding are the basis and reliability support for the motor design.

The complex structure and significant dimensional variations in motor windings make establishing an efficient and accurate thermal analysis model a key research focus and challenge. At present, the main methods for calculating the temperature field of the motor are numerical calculation method and analytical/semi-analytical method [1,2]. Numerical analysis methods encompass various techniques such as finite element [3], finite volume [4], and finite difference [5] methods. They have been widely used because of their advantages such as convenient processing, accurate calculation and visualization of

Check for updates

Academic Editor: Francisco Javier Ruiz-Rodríguez

Received: 22 April 2026
Revised: 19 May 2026
Accepted: 20 May 2026
Published: 27 May 2026

Copyright: © 2026 by the authors. Licensee MDPI, Basel, Switzerland. This article is an open access article distributed under the terms and conditions of the Creative Commons Attribution (CC BY) license.

results [6,7]. The difficulty and key to numerical computation methods lie in the efficient processing of computational models [8]. In the process of motor temperature calculation, the winding structure is the most complex, and the equivalent treatment of its thermal model is particularly critical, attracting extensive research from scholars.

The commonly used winding equivalent methods include the area weight method and multi-layer thermal resistance series method [9]. Early studies predominantly employed homogenization methods, treating windings as composite materials composed of copper wire and insulating materials, and calculating their equivalent thermal conductivity using analytical models [10]. The Hashin–Shtrikman and Milton models are widely used and studied [11,12], in which the Milton model takes into account the cylindrical microstructure of the conductor to predict the equivalent thermal conductivity more accurately. SHI [11] considered the uneven heating and temperature distribution inside the winding under fault conditions such as inter-turn short circuit, and verified that the lumped-parameter (LP) model is much more efficient than the three-dimensional (3-D) CFD model while ensuring accuracy, which is suitable for rapid thermal evaluation in the design stage. Further studies have revealed that equivalent models incorporating geometric correction factors [13] and accounting for filling factors and porosity [14,15] typically exhibit superior predictive accuracy compared with simple volume-weighted methods. The core of such methods lies in obtaining equivalent material parameters, thereby simplifying complex winding structures into a homogeneous heat-conducting body. While this greatly simplifies calculations, it struggles to capture temperature gradients generated within the windings, particularly under high current densities.

Meanwhile, the thermal circuit model is widely used because of its convenience in system-level simulation. In this kind of model, the LP thermal network is established by analyzing the winding structure and the temperature field of the motor is analyzed by combining the CFD model [16,17], or by comparing the copper conductor and the insulating material in the slot to the metal and gas in the porous structure respectively, the equivalent thermal conductivity is derived by the thermal resistance network method [18]. It provides an effective tool for rapid thermal evaluation and optimization of thermal management solutions during the initial design phase of electric motors.

To more accurately describe internal temperature distribution, layered thermal models (or multi-layer thermal resistance series method) have emerged. By dividing the winding into multiple copper layers and insulation layers, these models effectively reflect the temperature gradient within the slots. From the layered concept proposed by Staton [19], to the ‘elliptical stratification’ developed by Nategh [20] and the ‘segmentation-layer’ model for Litz wire windings [21], to the application and optimization of high power density motors and Litz wire windings by Liang [22] and Wrobel [23], this method significantly improves the accuracy of hot spot temperature prediction while maintaining high computational efficiency. Furthermore, the dynamic multilayer model proposed by Fan [24] can adaptively adjust layering strategies based on temperature distribution, achieving an optimized balance between accuracy and efficiency.

With the deepening of research, experimental calibration and multi-method comparisons become crucial for validating and enhancing model reliability. Boglietti systematically discussed the method of determining the key parameters in the thermal model of the motor [25]. Through the DC transient thermal test, the equivalent thermal parameters were derived from the change in winding resistance, revealing the significant influence of manufacturing process (especially the impregnation quality) on the thermal conductivity of the winding [25,26], and it was found that different winding types (such as fractional-slot-concentrated winding) will lead to multiple changes in the equivalent thermal conductivity due to structural differences [27]. Simpson [28] and Tang [29] systematically evaluated

the applicability of analytical methods, finite element methods, and computational fluid dynamics (CFD). It is generally recognized that the CFD method offers greater precision in parameter accuracy, while analytical methods are suitable for rapid estimation. In summary, research on the equivalent thermal model of motor windings has evolved from simplifications based solely on material properties to a comprehensive approach integrating experimental testing and theoretical modeling. However, equivalent thermal models for different winding configurations exhibit certain differences.

As an important winding topology, the random winding has become the preferred scheme considering both performance and economy because of its strong adaptability, good thermal distribution uniformity, and effective balance of loss and practicability through reasonable design [30,31]. The random winding is manufactured by multi-layer winding of enameled wire followed by varnish impregnation. It primarily consists of copper wire, enameled wire varnish, and impregnating varnish [32]. Due to the small dimensions of insulating materials (enameled wire varnish, impregnating varnish) relative to the diameter of copper conductors, modeling the entire structure in CFD simulation calculations would result in an excessively fine mesh partitioning for the temperature field calculation model. This leads to a dramatic increase in the number of mesh elements, significantly reducing computational efficiency.

Therefore, this paper conducts an in-depth study on the thermal model equivalent methods for the random winding, providing a detailed comparison of the advantages and disadvantages of the three approaches: concentrated equivalent, anisotropic equivalent, and layered equivalent. Firstly, a precise thermal model was established for a single-tooth sample of a specific permanent magnet motor, with detailed analysis of its temperature distribution characteristics. Using this model as a baseline, the principles and computational results of three typical equivalent methods—concentrated equivalent, anisotropic equivalent, and layered equivalent—were successively analyzed. A temperature test platform for single-tooth windings was constructed to validate the accuracy of the computational methods. Finally, the computational efficiency, accuracy, and applicability of the three methods are compared and discussed. It provides effective support and theoretical basis for the equivalent calculation of random winding thermal models, significantly enhancing the efficiency and accuracy of temperature calculations.

2. Contribution and Outline of the Paper

2.1. Contributions

To comprehensively resolve the trade-off between calculation accuracy and computational efficiency in motor temperature field simulations, the equivalent methods for the thermal model of random windings were studied in detail. Combined with a single-tooth winding temperature rise experimental platform, the advantages, disadvantages, and applicable scopes of different equivalent methods are thoroughly investigated. The main innovations are as follows:

(1) Aiming at the difficulty in equivalent thermal field modeling of random windings, two novel equivalent modeling strategies, namely the layered equivalent method and the anisotropic equivalent method, are proposed to simultaneously improve calculation accuracy and computational efficiency.
(2) Based on the fundamental principles of heat transfer, the anisotropic heat conduction mechanism of random windings is revealed. The basic thermal equivalent theory for random winding modeling is perfected, which further enriches the theoretical system of temperature field analysis for motor windings.
(3) A systematic analysis of different equivalent methods for winding thermal models is carried out from multiple perspectives, including equivalence principles, model

construction, mesh generation, computational accuracy, and simulation efficiency, clearly defining the applicable scopes and boundaries of each method.

(4) The proposed modeling methods and analysis framework can be directly applied to thermal design, temperature rise prediction and heat dissipation optimization of various motor windings, providing strong technical support for accurate and efficient temperature field calculation of motors with loose windings.

The proposed equivalent thermal modeling methods for motor windings in this paper are developed and parameterized under the precondition of healthy and fault-free operation, assuming a uniformly distributed heat source within the windings, intact insulation structure, and constant thermal properties. Therefore, this model is more suitable for rapid temperature field calculation under rated operation and healthy, slight overload conditions, but is not applicable for accurate temperature prediction under extreme fault conditions such as short circuits.

2.2. Outline

This paper proceeds as follows. Firstly, the research status and practical requirements of the winding equivalent thermal model are summarized. The third part clarifies the research object and calculation input benchmark of the article. The fourth part analyzes the concentrated equivalent method, anisotropic equivalent method and layered equivalent method of the thermal model of the random winding. In the fifth part, the temperature test under different operating conditions is conducted for the single tooth winding sample. In the sixth part, combined with the results of temperature test, the advantages and disadvantages of three equivalent methods are compared and analyzed. The seventh part is the summary and prospect.

3. Model and Theory Analysis

3.1. Analysis of the Random Winding Structure

In the numerical calculation of the motor temperature field, the winding structure is the most complex to construct and also serves as the core and key component for motor temperature rise analysis and temperature field modeling. To achieve refined thermal modeling of the winding region, directly establishing a full-machine model would significantly increase the geometric complexity and mesh size, substantially prolonging the simulation time and reducing numerical solution efficiency. Given the strict periodic symmetry of the motor's electromagnetic and structural characteristics, the winding and heat dissipation features of a single tooth can effectively represent the typical behavior of the entire motor. Therefore, to conserve computational resources and improve simulation efficiency, this paper selects the single-tooth winding as the research object and investigates the equivalent thermal modeling method for random-wound windings.

In this paper, the single-tooth winding of a random winding motor is selected for research. The main characteristic parameters and the stator slot geometry are provided in Table 1 and Figure 1, respectively. The single-tooth winding structure is mainly composed of iron core, winding, insulation bracket and other structures, as shown in Figure 2. The basic dimensions of the stator slot profile are shown in Table 2.

Table 1. Parameters of winding.

Parameters	Value
Stator core length (mm)	90
Slot type (mm)	Semi-closed slot
Winding wire gauge (mm)	1.12
Number of parallel windings at the root (M)	12

Table 1. *Cont.*

Parameters	Value
Number of turns per single coil (N)	16
Number of parallel branches in the winding	1
Cooling method	Air-cooled

Table 2. Parameters of slot.

Parameters	Value/mm	Parameters	Value/mm
bs0	10	hs0	2
bs1	29	hs1	3
bs2	34.2	hs2	21

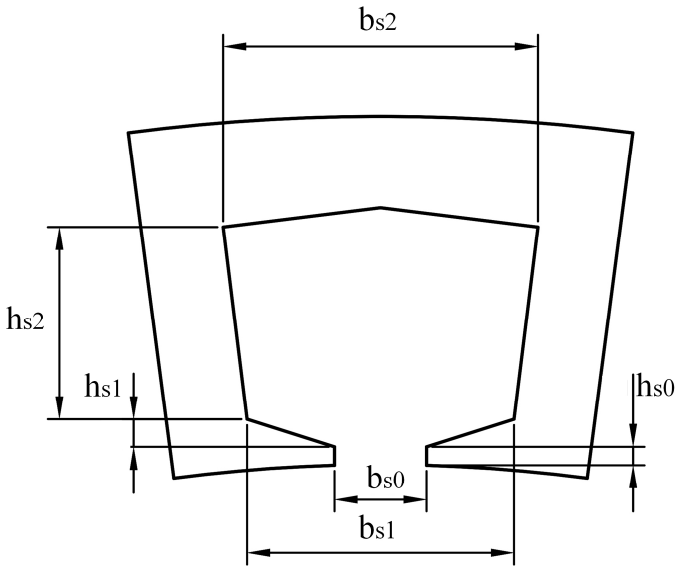

Figure 1. Slot structure.

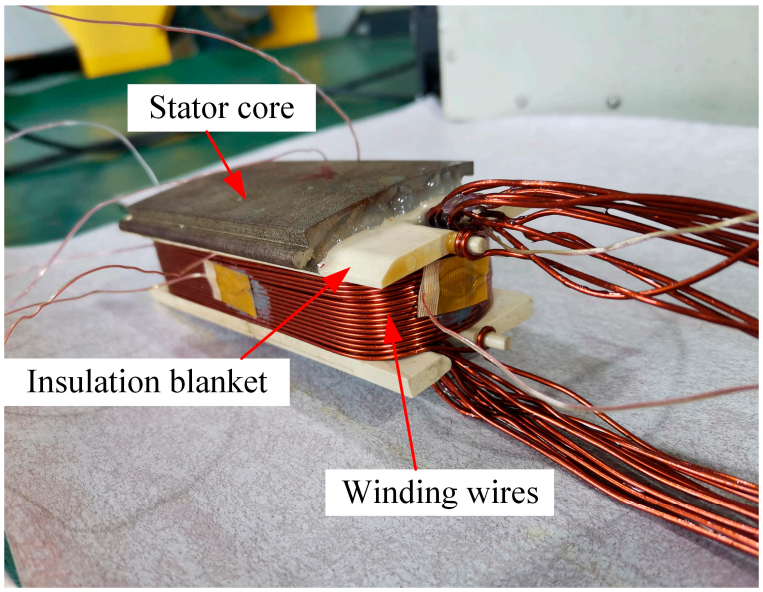

Figure 2. Single tooth winding.

3.2. Theoretical Basis

When the motor is running, heat generated within the windings is transferred through thermal conduction to the insulation varnish layer and the iron core. It is then dissipated into the surrounding air via thermal convection between the iron core surface and the external air, as well as through surface thermal radiation. Among these, heat conduction within solid components such as windings, insulating supports, and cores follows the heat conduction differential equation:

$$\rho c \frac{\partial T}{\partial \tau} = \frac{\partial}{\partial x}(\lambda \frac{\partial T}{\partial x}) + \frac{\partial}{\partial y}(\lambda \frac{\partial T}{\partial y}) + \frac{\partial}{\partial z}(\lambda \frac{\partial T}{\partial z}) + q_v \quad (1)$$

where ρ is the solid density, kg/m^3; c is the specific heat capacity, J/(kg·K); T is the temperature, K; τ is the time, s; x, y, z is the direction of the coordinate axis respectively; λ is the thermal conductivity, W/(m·K); and q_v is the heat source of the micro-element.

Convective heats transfer between cooling air and solid surfaces such as windings and cores follows Newton's law of heat transfer:

$$\phi = hA(T_w - T_f) \quad (2)$$

where ϕ represents the heat transfer rate, W; h represents the convective heat transfer coefficient, W/(m^2·K); A represents the heat transfer area, m^2; T_w represents the solid surface temperature, K; and T_f represents the fluid temperature, K.

The thermal radiation of solid surface follows the Stefan–Boltzmann law [33]:

$$\phi_1 = \varepsilon \sigma A(T_w^4 - T_f^4) \quad (3)$$

where ε is the emissivity of the solid, W/(m^2 · K); σ is the Stefan–Boltzmann constant (5.67×10^{-8} W/(m^2 · K^4)).

In this paper, the CFD analysis method based on fluid–solid coupling is used to simulate the flow field and temperature field of the motor. Although the internal flow field and heat transfer of the motor are complex, it still follows the N-S equation and the law of conservation of energy.

The flow of cooling air within the motor was solved using a model provided by Fluent 2022 R1. This model represents a closed system governed by the momentum conservation equation and the continuity equation [34,35].

$$\left.\begin{array}{l} \rho \frac{\partial U}{\partial t} - \nabla\left[\left(\eta + \rho C_\mu \frac{k^2}{\varepsilon}\right) \cdot \left(\nabla U + (\nabla U)^T\right)\right] + \rho U \cdot \nabla U + \nabla P = F \\ \nabla \cdot U = 0 \end{array}\right\} \quad (4)$$

where ρ is the fluid density, kg/m^3; μ is the dynamic viscosity, N · s/m^2; U is the mean velocity field; C_μ is an empirical constant; k is the turbulent kinetic energy; ε is the turbulent energy dissipation rate; P is the pressure, Pa; and F is the volume force vector.

By combining the above control equations, the temperature distribution characteristics of a single-tooth winding in an electric motor can be simulated and solved. The following basic assumptions and boundary conditions are set for the calculation:

(1) The cooling environment is consistent with the experimental conditions;
(2) Winding losses are treated as a uniform heat source, achieved by loading the heat source density;
(3) The interfaces between components are set as coupled interfaces.

3.3. Calculation Basis

In this paper, the numerical analysis method and the CFD method are used to compare the calculation methods of the equivalent thermal model of the random winding in detail. Firstly, according to the equivalent principle, the calculation parameters corresponding to different equivalent methods are obtained by numerical calculation method. Then, different CFD calculation models are established, and the temperature field is calculated by a fluent temperature field calculation module. In order to fully verify the advantages and disadvantages of different equivalent methods, the simulation calculations of steady-state and transient temperature fields are carried out respectively.

The single-tooth winding studied in this paper is part of the structure of a certain type of hundred-kilowatt permanent magnet propulsion motor. Its typical operating conditions include steady-state long-term operation and transient operation for 10 min. The calculation basis of the copper loss of the single-tooth winding is to ensure that the current density of the single-tooth winding is consistent with the two typical operating conditions of the prototype, and the copper loss of the single-tooth winding is calculated. In order to ensure that the calculation is consistent with the cooling conditions of the experiment, the ambient temperature used in the computations was set to match the real-time ambient temperature during the experiments, as shown in Table 3.

Table 3. Loss and boundary conditions.

Conditions	Copper loss	Ambient Temperature	Operating Time
Steady-state	54 W	25.2 °C	Long-term
Transient	154 W	27.1 °C	10 min

The parameters of each material are shown in Table 4.

Table 4. Material physical parameters.

Component	Density kg/m^3	Specific Heat Capacity J/(kg·K)	Thermal Conductivity W/(m·K)
Winding	8978	381	380
Stator core	7650	583	34/34/8.54
Insulation bracket	1310	1700	1.7
Insulation	2800	1300	0.2
Air	1.225	1006.43	0.0242

4. Analysis of Calculation Methods for Thermal Models of the Random Winding

4.1. Analysis of the Full Model

4.1.1. Geometric Model

The main structure of the stator single-tooth winding is composed of a stator core, an insulation bracket, copper wire, impregnating varnish, insulating varnish, etc., which exhibits left and right symmetry. Therefore, a 1/2 symmetrical full model is established. The single-tooth winding studied in this paper consists of 16 enameled wires with a diameter of 1.12 mm wound in parallel for 12 layers.

A complete model of all components is established as shown in Figure 3. The motor winding includes copper wire, insulating varnish, impregnating varnish, and air gaps, with the winding insulation and air gaps modeled as a unified entity. To improve the slot fill factor and reduce the gaps between windings, open-wound motors typically use fully automated winding and embedding equipment, which ensures that the enameled wire is arranged neatly and uniformly, with consistent layering, and allows for precise

control of the number of turns and the slot fill factor. It can effectively avoid the problems of artificial winding wiring disorder and insulation damage, improve the three-phase electromagnetic consistency, heat dissipation performance and insulation reliability, and ensure the operation quality and batch process stability of the motor. A partial structural diagram of the winding section is shown in Figure 4.

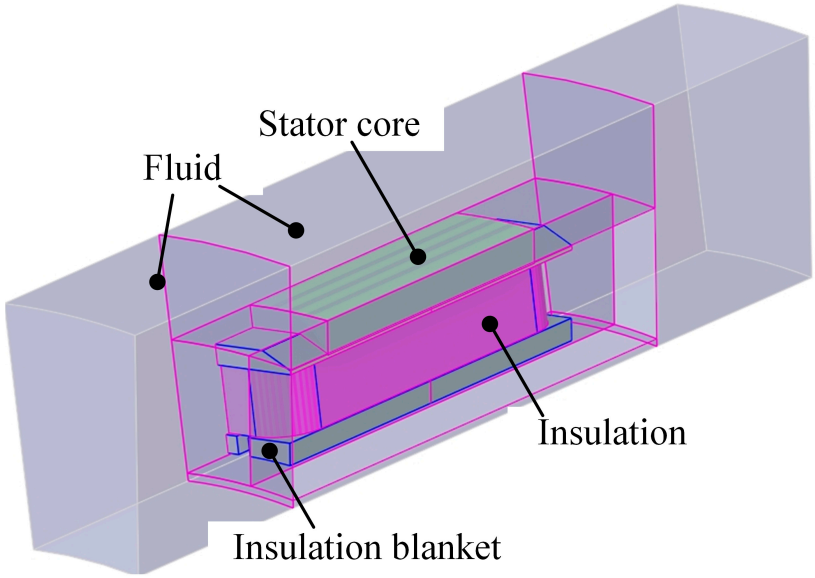

Figure 3. Full model.

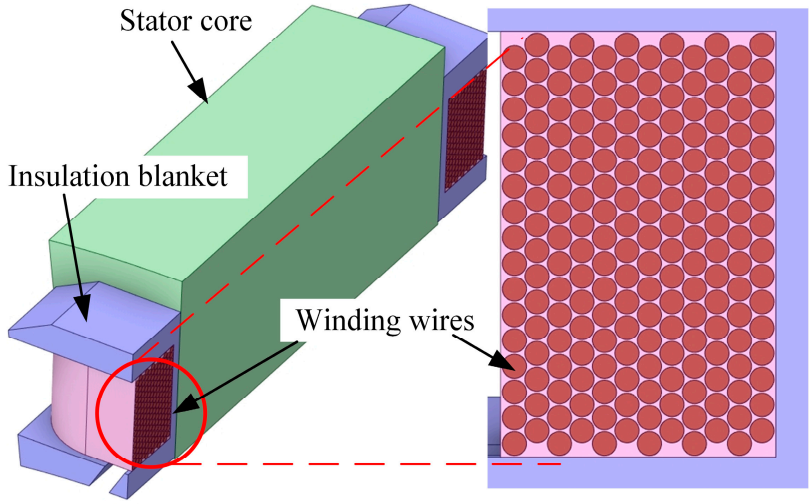

Figure 4. Detail structure.

The model is meshed by Fluent Meshing 2022 R1, and the smaller size positions such as copper wire and insulation material are encrypted. The model meshing results are shown in Figure 5. The details of the mesh results are shown in Table 5. The grid independence is verified before the calculation, as shown in Appendix A.

Table 5. The details of the full model meshing results.

Model	Mesh Count	Mesh Time	Minimum Orthogonal Quality
Full model	10,387,973	57.9 min	0.2317

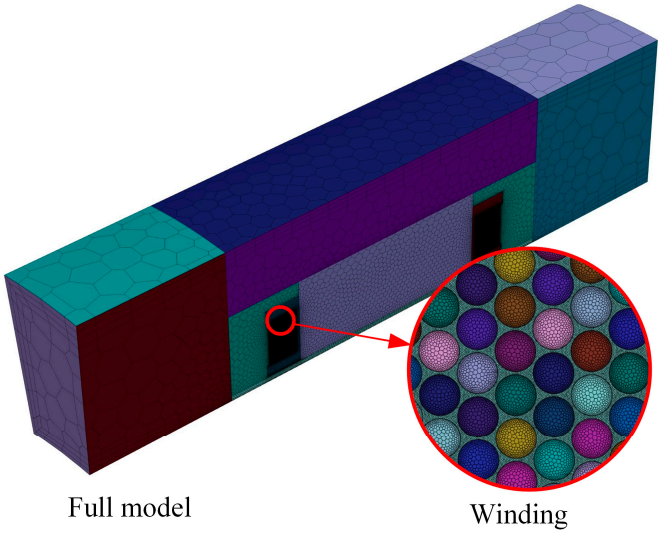

Figure 5. Mesh of full model.

4.1.2. Results

The temperature of the single-tooth winding under two operating conditions is calculated, and the temperature results of the winding are shown in Table 6. MaxTR represents maximum temperature rise and AveTR represents average temperature rise.

Table 6. Temperature results of the full model.

Conditions	MaxT/°C	AveT/°C	MaxTR/K	AveTR/K	Calculation Time/min
Steady-state	174.0	166.5	148.8	141.3	173.5
Transient (10 min)	223.8	208.0	196.7	180.9	149.7

After completing the steady-state condition calculations, the temperature distribution contour map of the winding cross-section is shown in Figure 6. Analysis of the temperature distribution contour map reveals that the temperature distribution exhibits a characteristic pattern of higher temperatures at the center and lower temperatures at the edges. The highest temperatures are primarily concentrated in the central portion of the winding, while the lowest temperatures are distributed at the winding end faces.

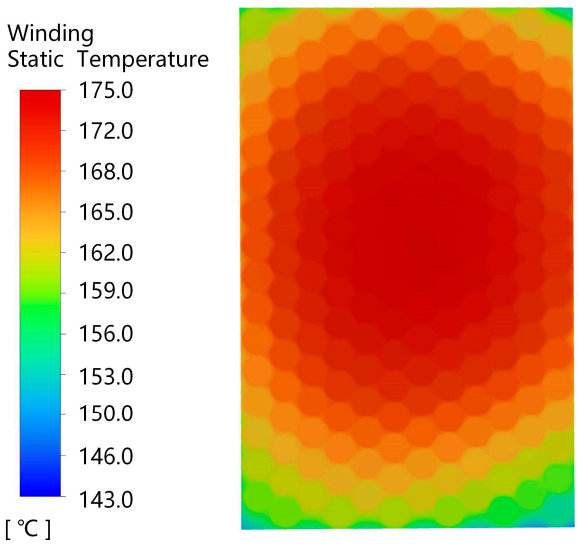

Figure 6. Temperature cloud diagram of winding section.

For transient operating conditions, to fully characterize the temperature distribution and variation patterns within the windings, temperature monitoring points were established at both the end face and center of the end windings. The temperature variation curves measured at various locations are presented in Figure 7.

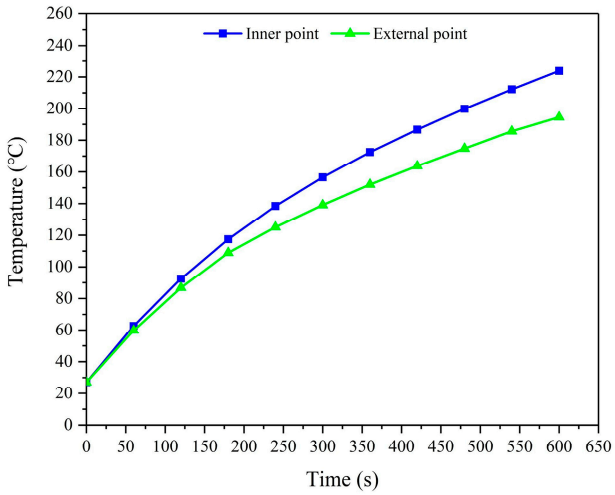

Figure 7. Temperature change diagram (transient).

Calculation results from the single-tooth winding full model indicate that despite establishing only a 1/2 single-slot model, the mesh count reaches 10 million. The model is complex and inefficient, rendering it unsuitable for computing intricate motor models.

Achieving efficient and accurate equivalent modeling for the random winding has become an urgent issue requiring resolution. The following sections will further compare and discuss the theoretical basis, equivalent methods, and computational results of various different equivalent approaches.

4.2. Concentrated Equivalent Method

The concentrated equivalent method is a typical application of the area-weighted approach. Its equivalent principle for motor windings involves approximating the insulation layer and windings based on the area contribution of each material along the heat transfer path. A schematic of the concentrated equivalent model is shown in Figure 8.

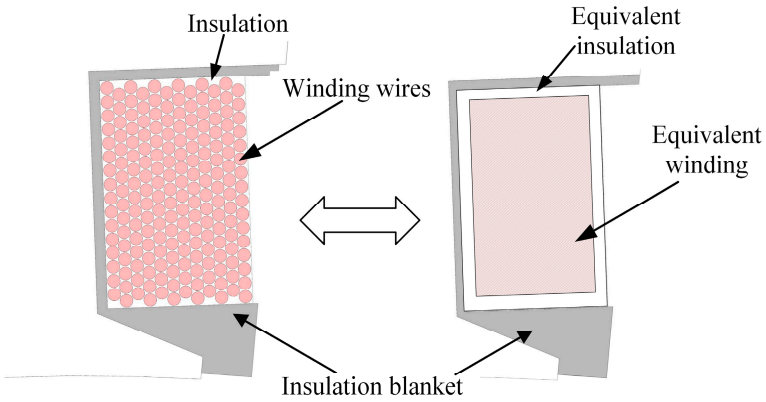

Figure 8. Concentrated equivalent diagram.

The key to the concentrated equivalent method is to determine the size of the equivalent winding and the equivalent insulation layer. For a stranded winding composed of N strands wound in parallel over M layers, the cross-sectional area of pure copper within a single tooth slot is:

$$A_{Cu} = \frac{\pi}{4} {D_w}^2 NM \tag{5}$$

The cross-sectional area of the single-groove winding insulation is:

$$A_{in} = \frac{\pi}{4} ({D_{in}}^2 - {D_w}^2) NM \tag{6}$$

The cross-sectional area of the single-groove winding impregnation varnish is:

$$A_q = \frac{\Delta m}{\rho_q l_w Z} \tag{7}$$

where the D_w is the diameter of pure copper, m; D_{in} the diameter of enameled wire, m; Δm is the mass difference before and after impregnation, kg; ρ_q is the density of impregnating varnish, kg/m^3; l_w is the axial length of a single slot winding, m; and Z is the number of slots in the motor.

When performing the concentrated equivalent method, the cross-sectional area of the equivalent winding and insulation shall remain consistent with the original model. The height and width of the equivalent winding shall satisfy the following relationship:

$$\begin{cases} A_{Cueq} = A_{Cu} \\ l_{j-cu} \times b_{j-cu} = A_{Cueq} \\ l_{j-cu} / b_{j-cu} = M/N \end{cases} \tag{8}$$

where the l_{j-cu}, b_{j-cu} represent the width and height of the equivalent winding, respectively, m.

The width and height of the equivalent insulation satisfy the following relationship:

$$\begin{cases} l_{j-in} \times b_{j-in} = A_{Cu} + A_q \\ l_{j-in} / b_{j-in} = M/N \end{cases} \tag{9}$$

where the l_{j-in}, b_{j-in} represent the width and height of the equivalent winding, respectively, m.

The parameters of the concentrated equivalent winding can be calculated from Equations (8) and (9), respectively, as shown in Table 7.

Table 7. Parameters of concentrated equivalent winding.

	Width/mm	Height/mm	Notes
Equivalent winding	11.9	15.8	-
Equivalent insulation	12.8	17.0	Winding included

Based on equivalent dimensional parameters, a concentrated equivalent model of a single-tooth winding is established as shown in Figure 9.

The model is meshed by Fluent Meshing software, and the model is encrypted at a small size position such as insulation material. The results of meshing are shown in Figure 10. The details of the mesh results are shown in Table 8.

Table 8. The details of the concentrated equivalent model meshing results.

Model	Mesh Count	Mesh Time	Minimum Orthogonal Quality
Concentrated equivalent model	1,642,444	3.3 min	0.2754

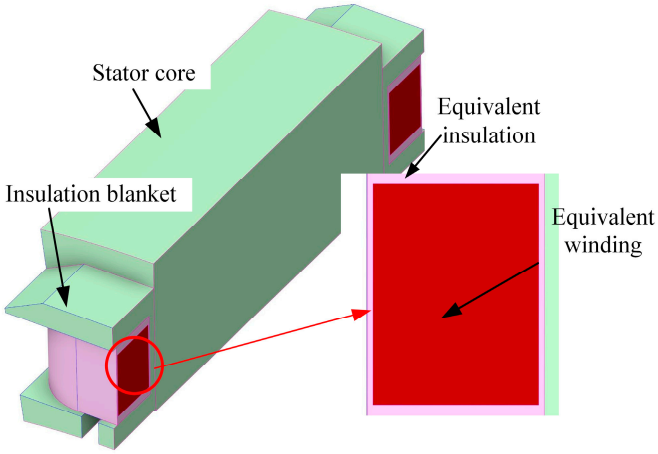

Figure 9. Concentrated equivalent winding model.

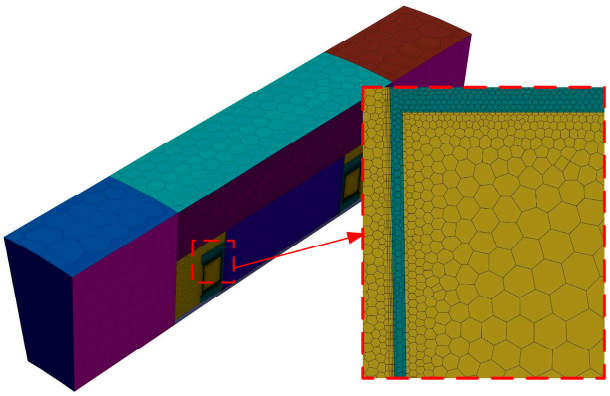

Figure 10. Mesh of concentrated equivalent winding.

The simulation calculation of the steady-state and transient temperature field is carried out by Fluent. The loss input and boundary condition setting are consistent with the full model, as shown in Tables 3 and 4.

The temperature results of the winding are shown in Table 9.

Table 9. Temperature results of the concentrated equivalent model.

Conditions	MaxT/°C	AveT/°C	MaxTR/K	AveTR/K	Calculation Time/min
Steady-state	174.8	174.7	149.6	149.5	53.9
Transient (10 min)	224.6	224.0	197.5	196.6	40.1

4.3. Layered Equivalent Method

According to the calculation temperature results of the full model, it is found that, as shown in Figure 6, the temperature distribution of the random winding can be approximated as multiple isothermal surfaces along the winding layers, and the winding can be modeled as multiple annular isothermal surfaces during calculation. The equivalent method is shown in Figure 11.

The layered equivalent method can be referenced from the lumped equivalent method, where the principle remains the same: the copper wire is the concentrated equivalent to the inside of the model, and the insulation layer is the concentrated equivalent to the periphery of the copper wire. The difference lies in the layered equivalent approach, which requires refining the equivalent of the winding to single-layer or multi-layer equivalences. The more layers, the higher the accuracy of the equivalent calculation.

In this paper, the single-tooth winding consists of 16 parallel-connected wires wound into 12 layers. The layered equivalent method adopts annular layering. To ensure accuracy,

each layer contains one turn of wire; after annular equivalence, the winding can be reduced to an equivalent of six layers. And layers 1–5 each contain one winding layer, and layer six contains 2 × 6 winding layers. Both the copper and insulation layer thicknesses in the equivalent model can be determined using the area-weighted method.

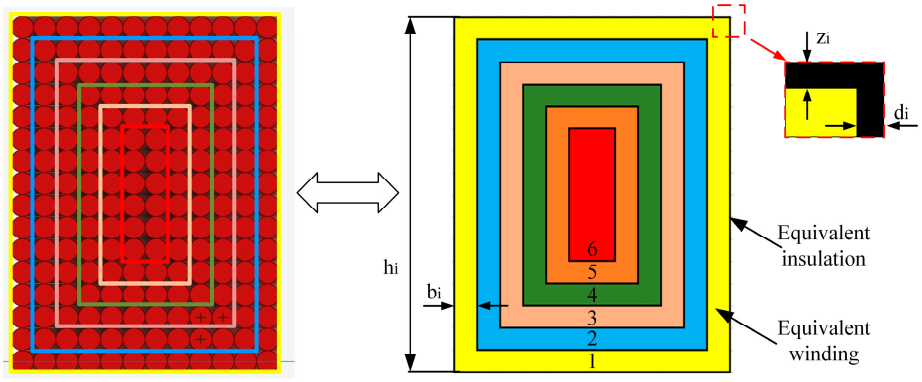

Figure 11. Layered equivalent diagram.

The thickness and height of the i-th equivalent winding and insulation layer are:

$$b_{\mathrm{i}} = n \times \frac{\sqrt{\pi {D_w}^2}}{2} \tag{10}$$

$$h_{\mathrm{i}} = m \times \frac{\sqrt{\pi {D_w}^2}}{2} \tag{11}$$

$$d_{\mathrm{i}} = n \times \left(\frac{\sqrt{\pi {D_{in}}^2}}{2} - b_{\mathrm{i}}\right) \tag{12}$$

$$z_{\mathrm{i}} = m \times \left(\frac{\sqrt{\pi {D_{in}}^2}}{2} - h_{\mathrm{i}}\right) \tag{13}$$

where the n and m denote the number of copper wires along the thickness and height directions, respectively, in the equivalent winding of the i-th layer.

According to the calculation results of Equations (10)–(13), the layered equivalent three-dimensional calculation model is established as shown in Figure 12.

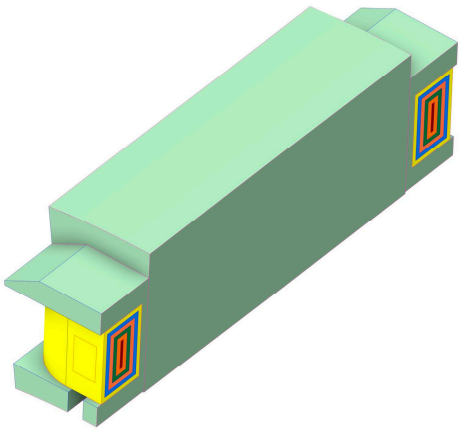

Figure 12. Layered equivalent model.

The model is meshed. Since the equivalent thickness of the single-layer insulation is only 0.2 mm, it is not modeled. During subsequent calculations, the contact surfaces between different layers are treated as walls with thickness. The wall thickness is set based

on calculation results, and the material is specified as insulation material. The results of meshing are shown in Figure 13. The details of the mesh results are shown in Table 10.

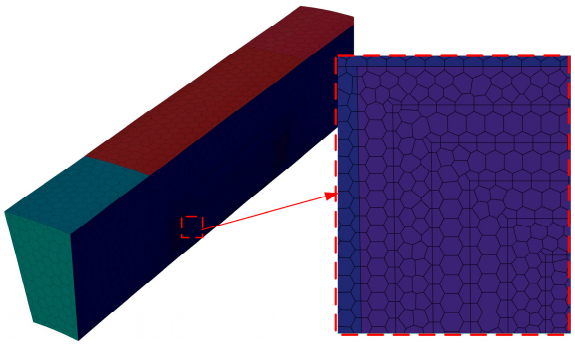

Figure 13. Mesh of layered equivalent model.

Table 10. The details of the layered equivalent model meshing results.

Model	Mesh Count	Mesh Time	Minimum Orthogonal Quality
Layered equivalent model	1,360,015	3.2 min	0.3

When the coupling model is simulated, the thermal conductivity of the equivalent winding layer is set to $\lambda_{cu} = 380\ \mathrm{W/(m \cdot K)}$, and the thermal conductivity of the equivalent insulation layer is set to $\lambda_{in} = 0.2\ \mathrm{W/(m \cdot K)}$. After iterative convergence, the temperature results of the single-tooth winding can be obtained as shown in Table 11.

Table 11. Temperature results of the layered equivalent model.

Conditions	MaxT/°C	AveT/°C	MaxTR/K	AveTR/K	Calculation Time/min
Steady-state	174.8	170.6	149.6	145.4	20.3
Transient (10 min)	223.1	215.3	196.0	182.7	25.9

4.4. Anisotropic Equivalent Method

The anisotropic equivalent method is based on the thermal resistance series method. The equivalent principle is to equate a variety of different materials to an equivalent body with anisotropy. In the process of temperature calculation, parameters such as the equivalent thermal conductivity, equivalent specific heat capacity, and equivalent density of the equivalent body must be determined.

Figure 14 shows the 3-D model for the anisotropic equivalent method of a single-slot winding.

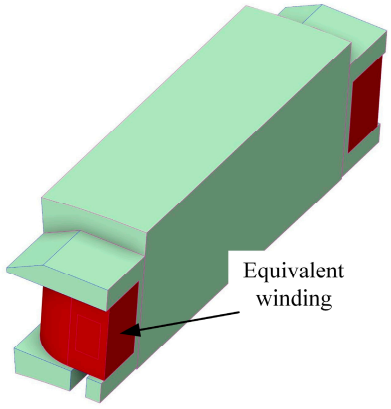

Figure 14. Anisotropic equivalent model.

4.4.1. Equivalent Thermal Conductivity

The stranded winding is formed by parallel winding multiple turns of several round conductors. The primary structure of the winding includes materials such as copper wire, insulation, and impregnating varnish. During motor manufacturing, mechanical winding is predominantly employed, resulting in a regular winding pattern that offers certain advantages for thermal conductivity equivalence. In this paper, based on the minimum resistance rule, the winding is equivalent by using the equivalent thermal resistance model, and the X, Y and Z directions (current direction) are considered respectively.

The thermal resistance equivalent principle of the winding along the X/Y section is shown in Figure 15.

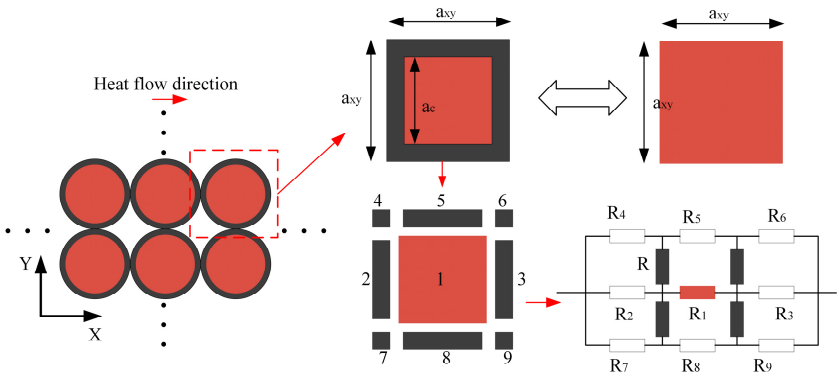

Figure 15. Thermal resistance equivalent model of single wire (X/Y).

The figure shows the equivalent processes of a single wire in the X and Y directions. The copper wire diameter is D_w, and the enameled wire diameter is D_{in}; the equivalent model dimensions are:

$$a_c = \frac{\sqrt{\pi {D_w}^2}}{2} \tag{14}$$

$$a_{xy} = \frac{\sqrt{\pi {D_{in}}^2}}{2} \tag{15}$$

The mathematical approximation method is used to calculate the equivalent thermal resistance under the assumptions of infinite and infinitesimal longitudinal thermal resistance, and the equivalent thermal resistance is obtained. As shown in Figure 16, the equivalent thermal path diagrams correspond to infinite and infinitesimal longitudinal thermal resistance, respectively.

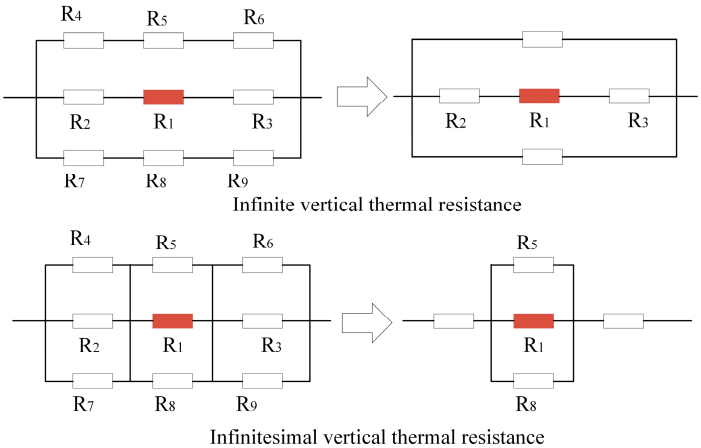

Figure 16. Thermal resistance equivalent diagram.

When the longitudinal thermal resistance is infinite:

$$R_1 = \frac{a_c}{a_c a_z \lambda_c} \tag{16}$$

$$R_2 = R_3 = \frac{0.5(a_{xy} - a_c)}{a_c a_z \lambda_{in}} \tag{17}$$

$$R' = \frac{a_{xy}}{0.5(a_{xy} - a_c) a_z \lambda_{in}} \tag{18}$$

The equivalent thermal resistance is:

$$R_{\max_i} = \left(\frac{1}{R'} + \frac{1}{R_1 + R_2 + R_3} + \frac{1}{R'} \right)^{-1} \tag{19}$$

The proportion of copper in the equivalent winding model is defined as:

$$\varepsilon = \frac{{a_c}^2}{{a_{xy}}^2} \tag{20}$$

Equation (19) can be further solved as:

$$R_{\max_i} = \frac{1}{a_{zi} \lambda_{in}} \cdot \frac{\lambda_{in} \sqrt{\varepsilon} + \lambda_c (1 - \sqrt{\varepsilon})}{\lambda_{in} \sqrt{\varepsilon} (1 - \sqrt{\varepsilon}) + \lambda_c (1 - \sqrt{\varepsilon})^2 + \lambda_c \sqrt{\varepsilon}} \tag{21}$$

where λ_{in} is the thermal conductivity of the insulating material, $\lambda_{in} = 0.2\ \mathrm{W/(m \cdot K)}$; λ_c is the thermal conductivity of copper, $\lambda_{cu} = 380\ \mathrm{W/(m \cdot K)}$.

When the longitudinal thermal resistance is infinitesimal:

$$R_5 = R_8 = \frac{a_c}{0.5(a_{xy} - a_c) a_z \lambda_{in}} \tag{22}$$

$$R'' = \frac{0.5(a_{xy} - a_c)}{a_{xy} a_z \lambda_{in}} \tag{23}$$

The equivalent thermal resistance is:

$$R_{\min_i} = R'' + \left(\frac{1}{R_5} + \frac{1}{R_1} + \frac{1}{R_8} \right)^{-1} + R'' \tag{24}$$

$$R_{\min_i} = \frac{1 - \sqrt{\varepsilon}}{a_{zi} \lambda_{in}} + \frac{\sqrt{\varepsilon}}{a_{zi} \lambda_{in} (1 - \sqrt{\varepsilon}) + a_{zi} \lambda_c \sqrt{\varepsilon}} \tag{25}$$

For a single wire, the equivalent thermal resistance in the X and Y directions is:

$$R_{eq_i} = \frac{R_{\min_i} + R_{\max_i}}{2} \tag{26}$$

Along the *Z*-axis direction of the winding (in the direction of current flow), the thermal resistance equivalent model for a single winding is shown in Figure 17.

The equivalent thermal resistance of each section of the winding along the *Z*-axis is as follows:

$$R_z = \frac{a_z}{{a_c}^2 \lambda_c} \tag{27}$$

$$R_{z1} = R_{z2} = \frac{a_z}{0.5({a_{xy}}^2 - {a_c}^2) \lambda_{in}} \tag{28}$$

Along the *Z*-axis direction, the equivalent thermal resistance of a single wire is:

$$R_{eqz_i} = \left(\frac{1}{R_{z1}} + \frac{1}{R_z} + \frac{1}{R_{z2}} \right)^{-1} \tag{29}$$

$$R_{eqz_i} = \frac{a_{zi}}{a_{xy}{}^2(\lambda_{in}(1-\varepsilon) + \lambda_c \varepsilon)} \tag{30}$$

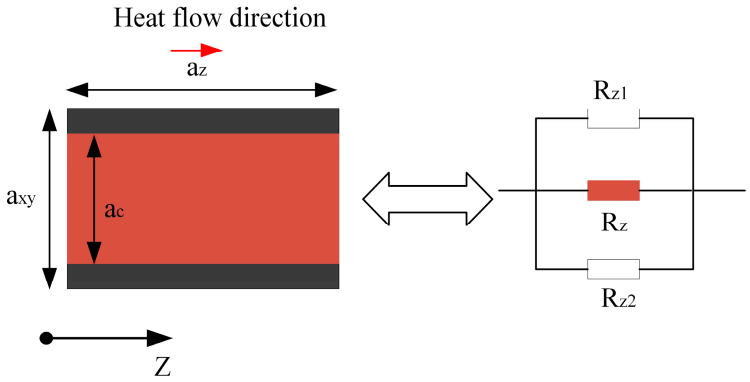

Figure 17. Thermal resistance equivalent model of single wire (Z).

Extending from a single wire to a single-tooth winding, the equivalent thermal resistance of the anisotropic equivalent winding model along the X, Y, and Z directions can be obtained as follows:

$$\begin{cases} R_{eqx} = \sum\limits_{i=1}^{M} R_{eq_i} \\ R_{eqy} = \sum\limits_{i=1}^{N} R_{eq_i} \\ R_{eqz} = \left(\sum\limits_{i=1}^{n} \dfrac{1}{R_{eqz_i}} \right)^{-1} \end{cases} \tag{31}$$

where the n is the number of wires per slot, $n = N \times M$.

For the subject of this study, the basic parameters are shown in Table 1. After equivalent calculation, the proportion of copper is 0.87. The equivalent thermal conductivity along different directions can be further calculated as: $\lambda_{eqx} = 3.8\ \mathrm{W/(m \cdot K)}$, $\lambda_{eqy} = 2.2\ \mathrm{W/(m \cdot K)}$, $\lambda_{eqz} = 284.1\ \mathrm{W/(m \cdot K)}$.

4.4.2. Equivalent Specific Heat Capacity

According to the formula for specific heat capacity [15]:

$$c_p = \frac{Q}{m \cdot \Delta T} \tag{32}$$

For the anisotropic equivalent models,

$$c_{p_eq} = \frac{\sum Q_i}{\sum m_i \cdot \Delta T} = \frac{(c_{cu} m_{cu} + c_{in} m_{in} + c_q \Delta m)\Delta T}{(m_{cu} + m_{in} + \Delta m)\Delta T} \tag{33}$$

where c_{cu}, c_{in}, and c_q represent the specific heat capacities of copper, insulation, and impregnating varnish, respectively. m_{cu}, m_{in}, and Δm represent the masses of copper, insulation, and impregnating varnish, respectively. For the subject of this study, the equivalent specific heat capacity is $c_{p_eq} = 435\ \mathrm{J/(kg \cdot K)}$.

4.4.3. Equivalent Density

The density calculation formula of a material is [15]:

$$\rho = \frac{m}{V} \tag{34}$$

For the anisotropic equivalent models,

$$\rho_{eq} = \frac{\sum m_i}{\sum V_i} \tag{35}$$

In this paper, the equivalent density is $\rho = 9055\ \mathrm{kg/m^3}$.

4.4.4. Results

The anisotropic equivalent model is meshed. The winding and insulating material are equivalent to an anisotropic uniform material, the fine structure such as enameled wire is eliminated, which greatly reduces the mesh amount of the calculation model and accelerates the mesh generation efficiency. The meshing results are shown in Figure 18. The details of the mesh results are shown in Table 12.

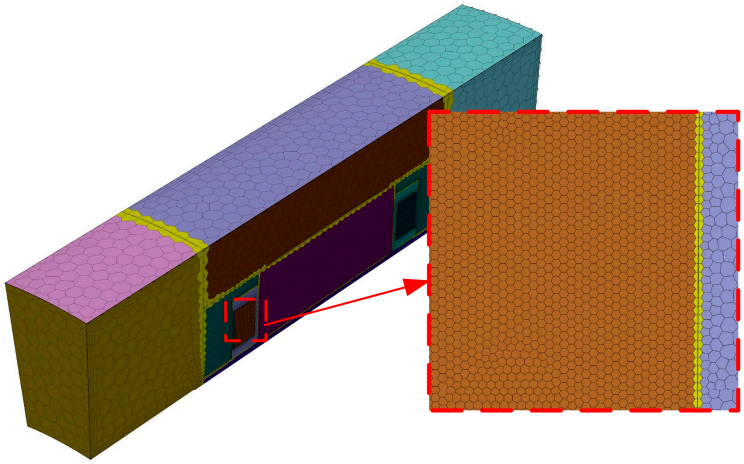

Figure 18. Mesh of anisotropic equivalent model.

Table 12. The details of the anisotropic equivalent model meshing results.

Model	Mesh Count	Mesh Time	Minimum Orthogonal Quality
Anisotropic equivalent model	287,074	1.0 min	0.3

After the iterative calculation converges, the temperature results of the single-tooth winding can be obtained as shown in Table 13.

Table 13. Temperature results of the anisotropic equivalent model.

Conditions	MaxT/°C	AveT/°C	MaxTR/K	AveTR/K	Calculation Time/min
Steady-state	174.3	168.3	149.1	143.1	24.1
Transient (10 min)	221.6	209.8	194.5	182.7	24.9

5. Experimental Verification

In order to fully verify the accuracy of different equivalent methods, a single-tooth winding sample was manufactured and a temperature test platform was built to verify the calculation results.

5.1. Experimental Platform

The experimental platform has two purposes. One is to precisely evaluate the winding temperature under different operating conditions, and the other is to test the temperature distribution characteristics at different positions of the same section of the winding. To achieve this, thermocouple temperature sensors are embedded in the winding end face and the middle position respectively, and the schematic diagram of the measuring point arrangement is shown in Figure 19.

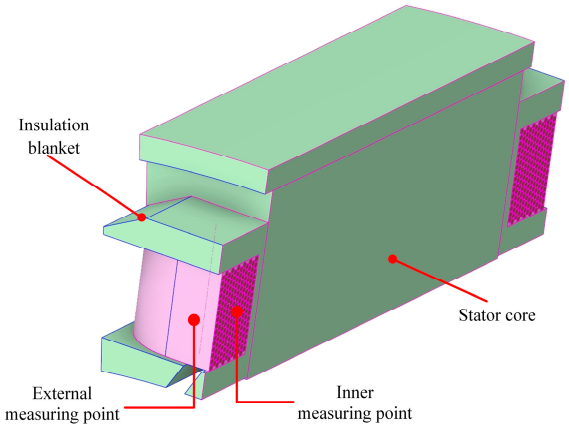

Figure 19. Diagram of measuring point arrangement.

The single-tooth winding temperature test platform is shown in Figure 20. The sample is wound by the machine, and the thermocouple temperature sensor is embedded in the winding process. The test platform is composed of DC power, temperature data logger, single-tooth winding sample, thermocouple sensor, data recording instrument and so on. The DC power supply provides constant power output, while the temperature data logger simultaneously acquires temperature readings from all measurement points.

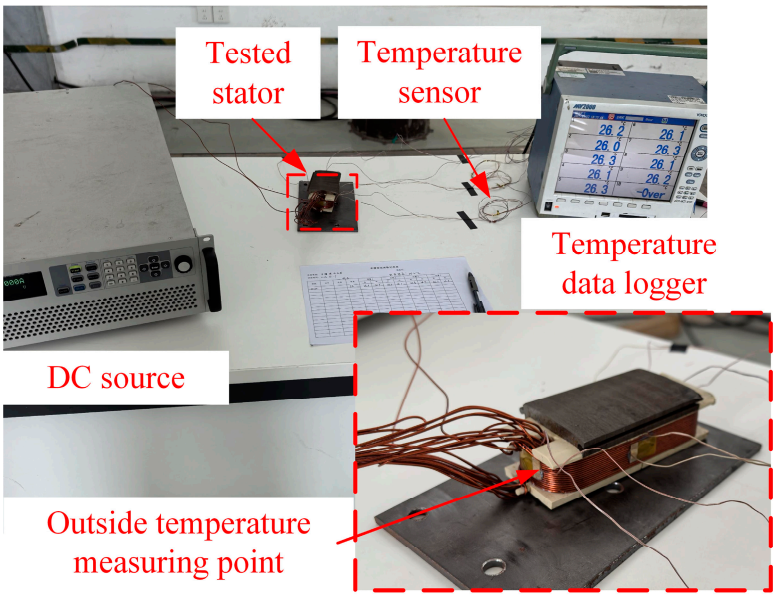

Figure 20. Temperature test platform.

During testing, both steady-state and transient operating condition temperature tests were conducted. A temperature data logger was used to record experimental data, with each test repeated twice to ensure data validity.

5.2. Experimental Results

The temperature results for the single-tooth winding under different operating conditions are shown in Table 14.

Table 14. Temperature results of test.

Conditions	Test Duration	Input Power/W	Inner Temp./°C	External Temp./°C
Steady-state	1 h 20 min	54	173.0	152.7
Transient	10 min	156	219.0	189.9

The temperature change curves for the inner and external points of the winding under two operating conditions are shown in Figure 21.

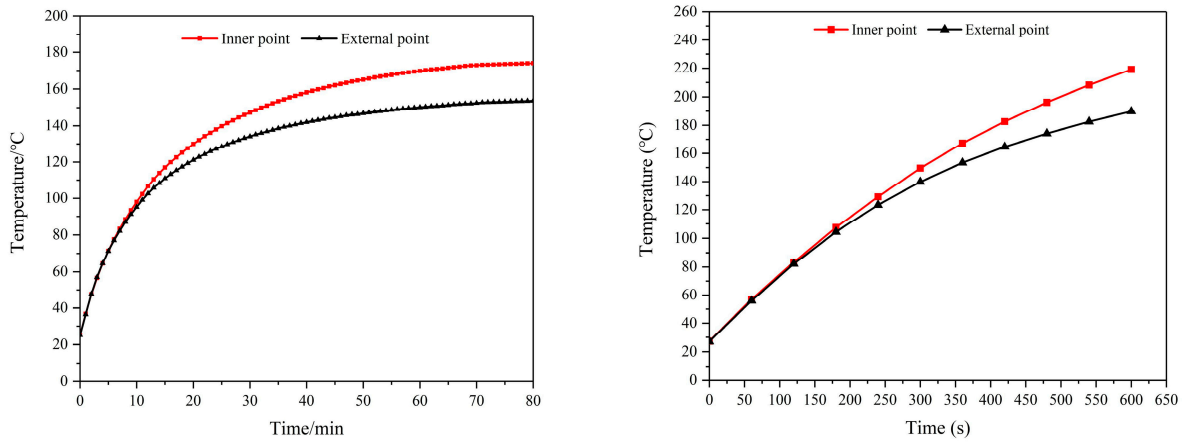

(**a**) (**b**)

Figure 21. Temperature change results(experiment). (**a**) Steady-state operating conditions; (**b**) transient operating condition.

Based on the experimental temperature results, a certain temperature difference exists between the inner and external point of the winding. The temperature rise is accompanied by a monotonic increase in the temperature difference between the two points. Under steady-state operating conditions, the temperature difference between the inner and external point is approximately 20.3 K. Under transient operating conditions, the AveT of the winding reaches 219.0 °C, with a temperature difference between the inner and external point of approximately 29.1 K.

6. Discussion and Analysis

During the motor design phase, different requirements exist for temperature field calculations. To clearly compare the applicability and advantages/disadvantages of various equivalent methods, detailed comparisons were conducted on the calculation results of four distinct thermal modeling analysis approaches, alongside comparative analysis with experimental results.

6.1. Comparison of Calculation Results

Figure 22 compares the calculation results of different equivalent methods with experimental data under steady-state operating conditions. It can be observed that at corresponding measurement points (internal and external points), the calculation results of all equivalent methods show good agreement with experimental results.

Table 15 lists the error comparisons between calculated and experimental results, with the maximum error being only 1.8%, occurring in the external measurement point results

of the layered equivalent method. The computational results fall within the permissible error range, demonstrating the validity of the equivalent methods.

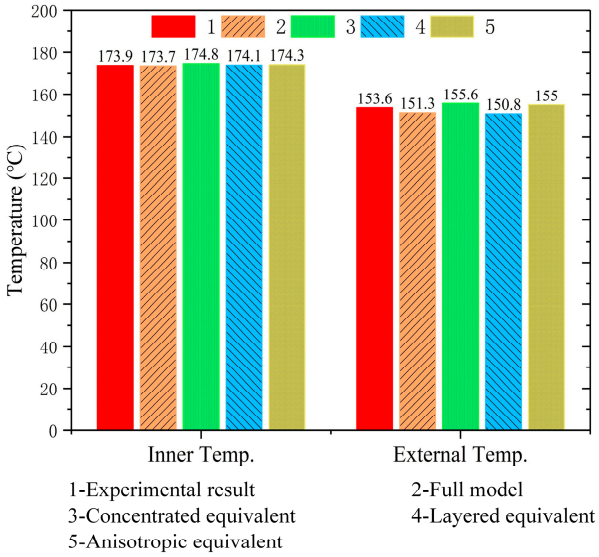

Figure 22. Temperature comparison of steady-state operating.

Table 15. Error comparison of steady-state operating.

Models	Temperature Error	
	Inner Point	External Point
Experimental results	Reference	Reference
Full model	0.1%	1.5%
Concentrated equivalent	0.5%	1.3%
Layered equivalent	0.1%	1.8%
Anisotropic equivalent	0.2%	0.9%

Under the transient conditions, the calculation results of the equivalent methods and the experimental are compared. As shown in Figure 23, the calculation results are in good agreement with the experimental results at the corresponding measuring points (internal points and external points).

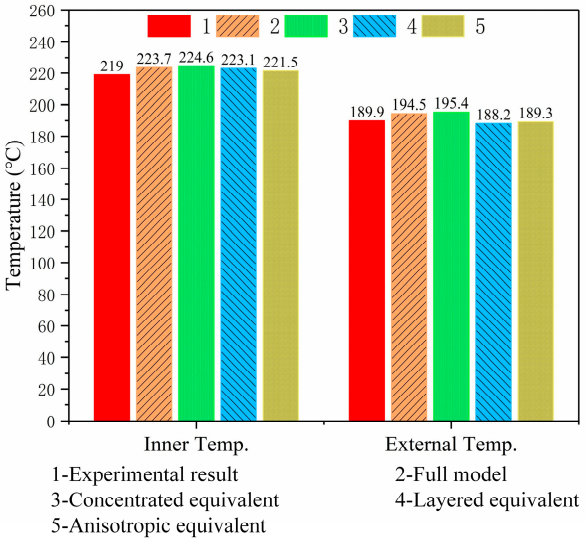

Figure 23. Comparison of final temperature under transient operating.

Table 16 compares the errors between the calculated and experimental results. The maximum error is the calculation result of the concentrated equivalent method, and the maximum error reaches 2.9%.

Table 16. Error comparison of transient operating.

Models	Temperature Error	
	Inner Point	External Point
Experimental results	Reference	Reference
Full model	2.1%	2.4%
Concentrated equivalent	2.6%	2.9%
Layered equivalent	1.9%	0.9%
Anisotropic equivalent	1.1%	0.3%

For transient operating conditions, it is also crucial to focus on temperature variations during operation. Therefore, the dynamic temperature changes from equivalent models were compared. Figure 24 contrasts the calculated temperature variations at internal and external measurement points with experimental results. Over a 10 min operating period, the temperature trends of the internal points calculated by the equivalent methods generally align with the experimental results. However, there are some differences between the calculation and the test results. The calculation results of the layered equivalent and the anisotropic equivalent method are lower, with the maximum deviation at the same time point (120 s) being approximately 6.8 K (anisotropic equivalent), but the overall trend is consistent. At the end of the transient operation, the maximum error of the temperature measuring point is only 2.9% (concentrated equivalent), which is within the allowable error range.

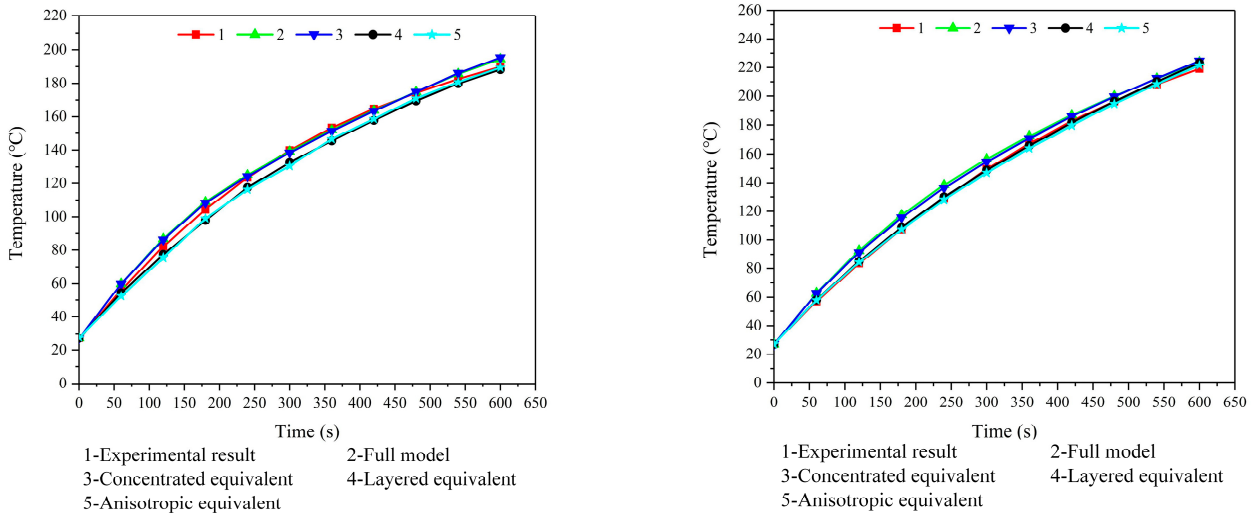

Figure 24. Temperature comparison of transient operating. (**a**) Inner measurement point; (**b**) external measurement point.

By comparing the computational and experimental results of two different operating conditions, it is proved that the four different equivalent methods have high accuracy in the calculation of the highest temperature of the winding, which shows the effectiveness of the equivalent method.

6.2. Comparison of Temperature Distribution

In order to further compare the calculation results of the four methods, the temperature distribution contours of the winding under the steady-state and transient conditions are drawn respectively, as shown in Figure 25.

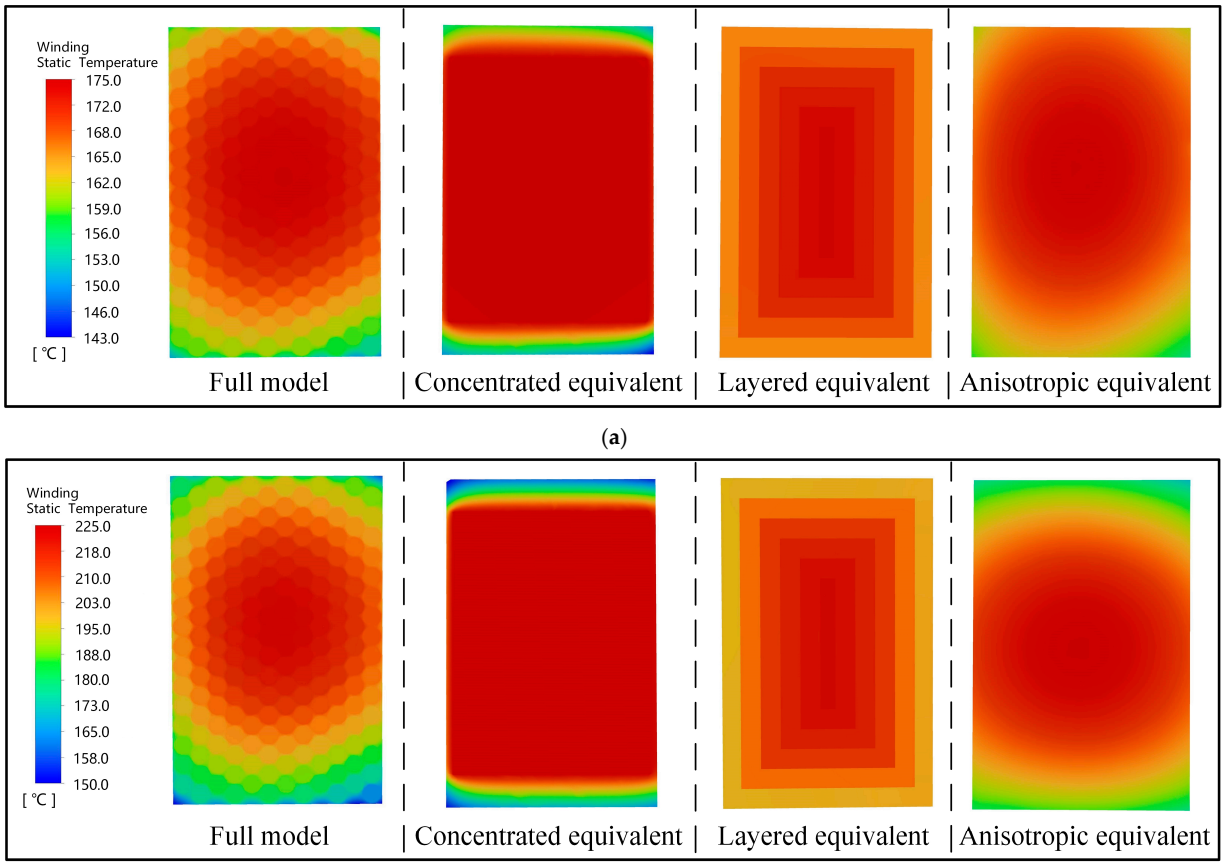

Figure 25. Comparison of temperature cloud map. (**a**) Temperature cloud distribution under steady-state conditions; (**b**) temperature cloud distribution under transient conditions.

The accuracy of the temperature calculation results has been compared in the preceding section. Now, using the full model's calculation results as the baseline, the temperature distribution contour plots of the winding is compared.

It can be observed that although the maximum winding temperatures calculated by the three equivalent methods exhibit high accuracy, significant differences exist in the temperature distribution of the windings. For the concentrated equivalent model, the temperature inside the winding is characterized by the highest temperature as a whole, and the temperature distribution of the winding is relatively concentrated, have no gradient characteristics. This indicates that the concentrated equivalent method can only estimate the AveT, lacks reliability in calculating the AveT, and cannot accurately describe the temperature distribution characteristics of the winding.

For the layered equivalent method, its temperature contour shows a distinct gradient distribution, which can describe the temperature distribution characteristics of the winding to a certain extent. However, discrepancies also exist in the depiction of some colder local areas.

For the anisotropic equivalent method, the temperature distribution characteristics are in good agreement with the full model, and the AveT calculation results have the smallest error compared with the full model. The MaxT and AveT comparison results are shown in Tables 17 and 18.

Table 17. Comparison of simulation and experimental winding temperature (steady).

Models	MaxT/°C	Error	AveT/°C	Error
Full model	174.0	Reference	166.5	Reference
Concentrated equivalent	174.8	0.5%	174.7	4.9%
Layered equivalent	174.8	0.5%	170.6	2.4%
Anisotropic equivalent	174.3	0.1%	168.3	1.1%

Table 18. Comparison of simulation and experimental winding temperature (transient).

Models	MaxT/°C	Error	AveT/°C	Error
Full model	223.8	Reference	208.0	Reference
Concentrated equivalent	224.6	0.3%	224.0	7.7%
Layered equivalent	223.1	0.3%	215.3	3.5%
Anisotropic equivalent	221.6	1.0%	209.8	0.9%

6.3. Comparison of Computational Efficiency

Computational efficiency is also a critical factor that must be considered. The overall time consumption for the meshing and simulating of four different methods under steady-state and transient conditions is summarized in Figure 26. To ensure consistency, we used the same computer for all calculations.

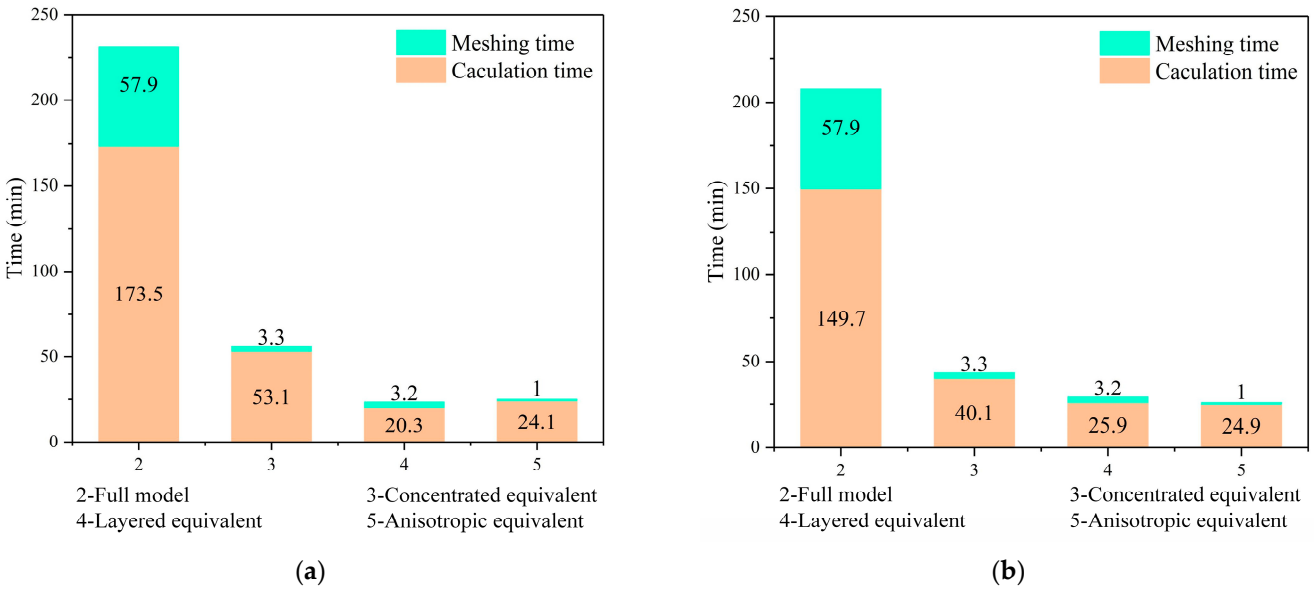

Figure 26. Comparison of computational time. (**a**) Steady-state operating conditions; (**b**) transient operating conditions.

It can be seen that under the two different operating conditions, the full model took the longest time, about 231.4 min and 207.6 min respectively. The concentrated equivalent model required moderate time, about 56.4 min and 43.3 min respectively. The layered equivalent model took 23.5 min and 29.1 min respectively. While the anisotropic equivalent thermal model took 25.1 min and 25.9 min respectively. Overall, the anisotropic and layered equivalent models took nearly the same time, which is only one-tenth of the full

model. Both of the anisotropic and layered equivalent methods are substantially more computationally efficient.

6.4. Summary

Through the detailed analysis and comparison of the calculation results of different thermal models, the following conclusions can be drawn:

1. In terms of the accuracy of temperature calculation results. The three equivalent thermal models demonstrate strong correlation with the experimental temperature measurements, which proves the validity of the model;
2. In terms of the winding temperature distribution characteristics. The anisotropic equivalent thermal model showed the highest agreement with the full model, with a maximum AveT error of only 1.1%. The concentrated equivalent thermal model exhibits the largest error at 7.7%, while the error of the layered equivalent thermal model is 2.4%;
3. In terms of the calculation efficiency. Compared with the full model, the three equivalent methods can greatly improve calculation efficiency. The max number of grids is only 15% of the full model, and the calculation time is shortened by about 75%;
4. However, the theoretical calculation process for the equivalent parameters in the anisotropic equivalent method is complex and computationally cumbersome, making it well-suited for detailed studies of winding temperature. In contrast, the layered equivalent method involves simpler equivalent parameter calculations, making it more applicable for engineering applications. It effectively captures temperature distribution characteristics while significantly enhancing computational efficiency.
5. The concentrated equivalent thermal model exhibits high accuracy in calculating the highest temperature, but it shows less accuracy in the AveT and temperature distribution characteristics. The maximum error in AveT reaches 7.7%. Therefore, it is more suitable for preliminary temperature field assessments during the motor design phase.

7. Conclusions and Prospects

7.1. Conclusions

Aiming to improve the accuracy of motor temperature field prediction, this research explores thermal modeling strategies for random windings. A critical analysis of concentrated and anisotropic equivalent methods is conducted, leading to the proposal of an enhanced layered equivalent method. Finally, four distinct thermal models were constructed, and their computational performance under steady-state and transient conditions was compared in detail. The conclusions reached are as follows:

1. The experimental results validate the high accuracy of all three equivalent thermal models, with relative errors all below 2.9%, while improving computational efficiency by at least 75% over the full model. The concentrated equivalent model exhibits the largest error, recording a deviation of only 2.9%;
2. The anisotropic equivalent thermal model demonstrates superior performance in depicting temperature distribution characteristics and computational efficiency. But the calculation of its equivalent parameters is complex;
3. The layered equivalent method provides a simple modeling principle, high computational efficiency, and accurate predictions of key temperature (maximum and average). However, it shows limitations in accurately depicting the temperature distribution characteristics of windings;
4. The concentrated equivalent thermal model is characterized by the simplest modeling principle and moderate computational efficiency, and can accurately calculate the

MaxT. It is suitable for preliminary temperature assessments during the initial stages of motor design.

In this paper, the calculation results of different equivalent thermal models are compared and verified by using single-tooth samples, which confirms the effectiveness of the proposed method. However, there are more factors to be considered in the motor system, and the temperature rise test of the motor system needs to be further verified to further improve the equivalent strategy.

7.2. Prospects

To fill the existing research gaps and make up for the deficiencies of current simplified models, we have formulated systematic follow-up research plans as follows.

1. Extending the equivalent models to a complete motor setup and validating the methods against experimental results from engineering motors;
2. Applying the equivalent method to other winding types, such as formed windings and hairpin windings;
3. Take influencing factors such as manufacturing processes and actual material properties into consideration when determining the equivalent parameters;
4. Using temperature rise data from engineering prototypes combined with artificial intelligence (AI) methods to calibrate equivalent parameters for higher accuracy, as well as developing AI-based winding temperature prediction models to greatly improve computational efficiency.

Author Contributions: Z.C.: Writing, review and editing, Data reduction, Conceptualization, Experimental verification. Z.Y.: Review, Data reduction, Conceptualization, Supervision, J.Y.: Motor design and loss calculation, Review, J.F.: Review and editing. All authors have read and agreed to the published version of the manuscript.

Funding: This work was supported by the National Natural Science Foundation of China under grant no. 52077217, and the National Key Laboratory of Electromagnetic Energy under grant no.61422172220202, and the Graduate Student Cooperative Research Project under grant no.202500030.

Data Availability Statement: Data will be made available on request.

Conflicts of Interest: The authors declare no conflicts of interest.

Appendix A. Grid Independence Verification

To ensure the reliability of the numerical results, the calculation grids with different density are divided, and the highest temperature of winding is used as the evaluation index to verify the grid independence. During the mesh generation process, computational meshes of varying densities were created by adjusting the minimum mesh size of critical components such as the windings. The highest temperature of the windings was used as the evaluation metric. The results are shown in following:

It can be seen that when the grid quantity is greater than 10,387,973 (full model), 1,642,444 (concentrated equivalent model), 1,360,015 (layered equivalent model), 287,074 (anisotropic equivalent model), the temperature calculation results of each component of the motor remain basically unchanged. The variation in the grid volume has a small effect on the temperature rise in the motor.

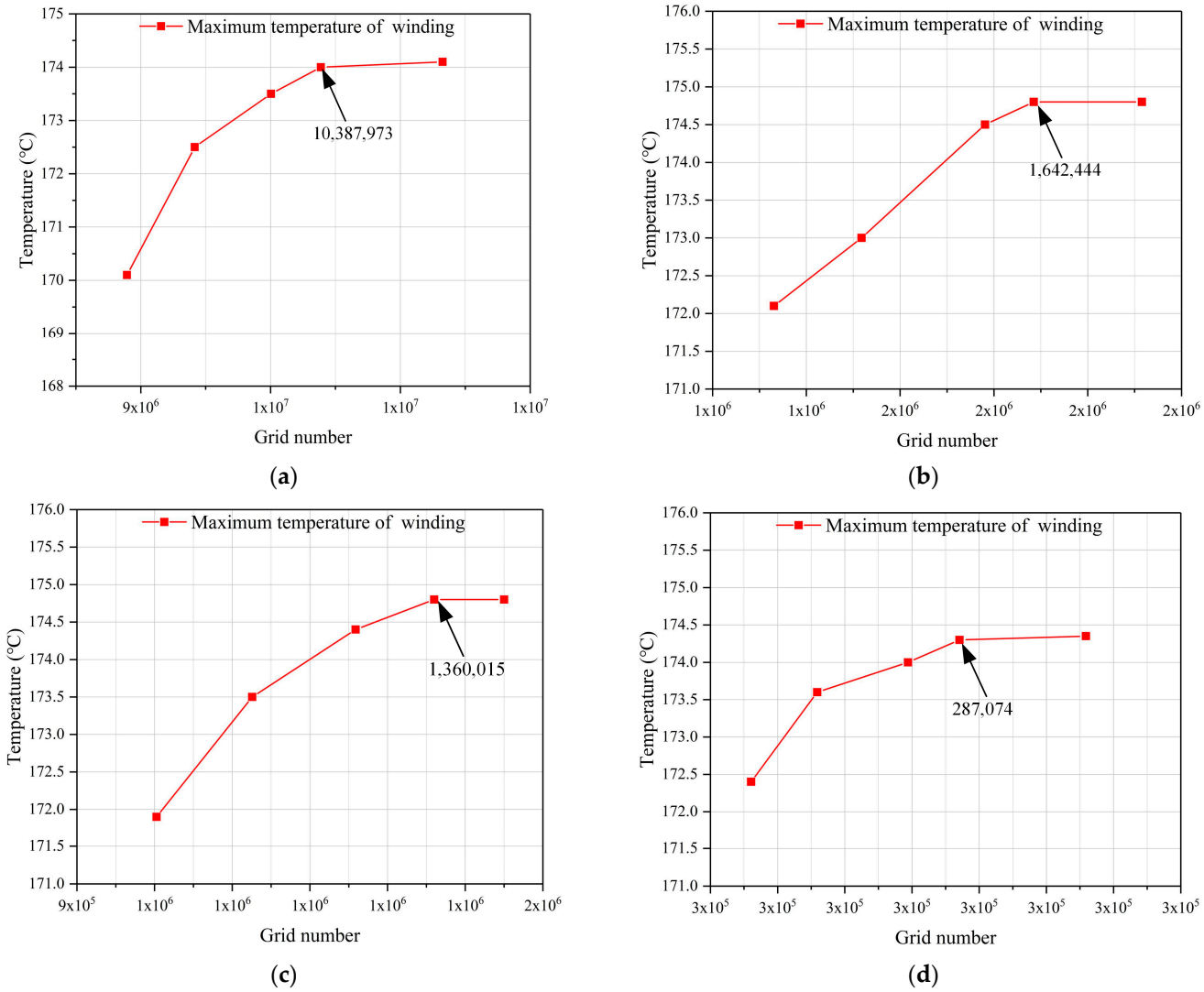

Figure A1. Grid independence verification. (**a**) Full model; (**b**) concentrated equivalent model; (**c**) layered equivalent model; (**d**) anisotropic equivalent model.

References

1. Rostami, N.; Feyzi, M.R.; Pyrhonen, J. Lumped-parameter thermal model for axial flux permanent magnet machines. *IEEE Trans. Magn.* **2012**, *49*, 1178–1184. [CrossRef]
2. Zhang, C.M.; Zhang, X.T.; Zhao, F. Improvements on permanent magnet synchronous motor by integrating heat pipes into windings for solar unmanned aerial vehicle. *Green Energy Intell. Transp.* **2022**, *1*, 100011. [CrossRef]
3. Grabowski, M.; Urbaniec, K.; Wernik, J. Numerical simulation and experimental verification of heat transfer from a finned housing of an electric motor. *Energy Convers. Manag.* **2016**, *125*, 91–96. [CrossRef]
4. Lu, Q.F.; Zhang, X.M.; Chen, Y. Modeling and investigation of thermal characteristics of a water-cooled permanent-magnet linear motor. *IEEE Trans. Ind. Appl.* **2014**, *51*, 2086–2096. [CrossRef]
5. Montonen, J.; Nerg, J.; Polikarpova, M. Integration principles and thermal analysis of an oil-cooled and-lubricated permanent magnet motor planetary gearbox drive system. *IEEE Access* **2019**, *7*, 69108–69118. [CrossRef]
6. Tang, C.Q.; Yu, Z.J.; Fu, J. Temperature field analysis of an air-water composite cooling high-speed generator. *Case Stud. Therm. Eng.* **2025**, *65*, 105646. [CrossRef]
7. Galloni, E.; Parisi, P.; Marignetti, F. CFD analyses of a radial fan for electric motor cooling. *Therm. Sci. Eng. Prog.* **2018**, *8*, 470–476. [CrossRef]
8. Gundabattini, E.; Mystkowski, A. Review of air-cooling strategies, combinations and thermal analysis (experimental and analytical) of a permanent magnet synchronous motor. *Proc. Inst. Mech. Eng. Part C J. Mech. Eng. Sci.* **2022**, *236*, 655–668. [CrossRef]

9. Tang, Y.; Chen, L.; Chai, F. Thermal modeling and analysis of active and end windings of enclosed permanent-magnet synchronous in-wheel motor based on multi-block method. *IEEE Trans. Energy Convers.* **2019**, *35*, 85–94. [CrossRef]
10. Idoughi, L.; Mininger, X.; Bouillault, F. Thermal model with winding homogenization and FIT discretization for stator slot. *IEEE Trans. Magn.* **2011**, *47*, 4822–4826. [CrossRef]
11. Shi, Y.W.; Wang, J.B.; Wang, B. Transient 3D lumped parameter and 3D FE thermal models of a PMASynRM under fault conditions with asymmetric temperature distribution. *IEEE Trans. Ind. Electron.* **2020**, *68*, 4623–4633. [CrossRef]
12. Tikadar, A.; Johnston, D.; Kumar, N. Comparison of electro-thermal performance of advanced cooling techniques for electric vehicle motors. *Appl. Therm. Eng.* **2021**, *183*, 116182. [CrossRef]
13. Zhang, X.; Dong, T.; Zhou, F. Equivalent Thermal Conductivity Estimation for Compact Electromagnetic Windings. *IEEE Trans. Ind. Electron.* **2019**, *66*, 6210–6219. [CrossRef]
14. Huang, X.Z.; Tan, Q.; Li, L.Y. Winding temperature field model considering void ratio and temperature rise of a permanent-magnet synchronous motor with high current density. *IEEE Trans. Ind. Electron.* **2016**, *64*, 2168–2177. [CrossRef]
15. Geng, W.; Zhiqiang, L.; Renjing, G.; Cao, T. An equivalent winding thermal model considering fill factor and void ratio for multi-physics coupling analysis of permanent magnet linear motors. *Appl. Therm. Eng.* **2024**, *236*, 121605. [CrossRef]
16. Galea, M.; Gerada, C.; Raminosoa, T. A thermal improvement technique for the phase windings of electrical machines. *IEEE Trans. Ind. Appl.* **2011**, *48*, 79–87. [CrossRef]
17. Le, L.H.T.; Messine, F.; Hénaux, C. 3D Electromagnetic and thermal analysis for an optimized wound rotor synchronous machine. In *Proceedings of the 2018 XIII International Conference on Electrical Machines (ICEM)*; IEEE: Alexandroupoli, Greece, 2018; pp. 455–460. [CrossRef]
18. Liu, X.M.; Yu, H.T.; Shi, Z.C. Porous metal model for calculating slot thermal conductivity coefficient of electric machines. *Appl. Therm. Eng.* **2017**, *111*, 981–988. [CrossRef]
19. Staton, D.; Boglietti, A.; Cavagnino, A. Solving the more difficult aspects of electric motor thermal analysis in small and medium size industrial induction motors. *IEEE Trans. Energy Convers.* **2005**, *20*, 620–628. [CrossRef]
20. Nategh, S.; Wallmark, O.; Leksell, M. Thermal analysis of a PMaSRM using partial FEA and lumped parameter modeling. *IEEE Trans. Energy Convers.* **2012**, *27*, 477–488. [CrossRef]
21. Nategh, S.; Øvrebø, S.; Mahdavi, S. Thermal modeling of a permanent magnet machine built using Litz wire. In *Proceedings of the 2015 International Conference on Electrical Systems for Aircraft, Railway, Ship Propulsion and Road Vehicles (ESARS)*; IEEE: Aachen, Germany, 2015; pp. 1–6. [CrossRef]
22. Liang, P.X.; Pei, Y.L.; Chai, F. Equivalent stator slot model of temperature field for high torque-density permanent magnet synchronous in-wheel motors accounting for winding type. *COMPEL Int. J. Comput. Math. Electr. Electron. Eng.* **2016**, *35*, 713–772. [CrossRef]
23. Wrobel, R.; Ayat, R.; Baker, J.L. Analytical methods for estimating equivalent thermal conductivity in impregnated electrical windings formed using Litz wire. In *Proceedings of the 2017 IEEE International Electric Machines and Drives Conference (IEMDC)*; IEEE: Miami, FL, USA, 2017; pp. 1–8. [CrossRef]
24. Fan, X.G.; Li, D.W.; Qu, R.H. A dynamic multilayer winding thermal model for electrical machines with concentrated windings. *IEEE Trans. Ind. Electron.* **2018**, *66*, 6189–6199. [CrossRef]
25. Boglietti, A.; Cavagnino, A.; Staton, D. Determination of critical parameters in electrical machine thermal models. *IEEE Trans. Ind. Appl.* **2008**, *44*, 1150–1159. [CrossRef]
26. Boglietti, A.; Carpaneto, E.; Cossale, M. Stator winding thermal conductivity evaluation: An industrial production assessment. *IEEE Trans. Ind. Appl.* **2016**, *52*, 3893–3900. [CrossRef]
27. Boglietti, A.; Cossale, M.; Vaschetto, S. Thermal conductivity evaluation of fractional-slot concentrated-winding machines. *IEEE Trans. Ind. Appl.* **2017**, *53*, 2059–2065. [CrossRef]
28. Simpson, N.; Wrobel, R.; Mellor, P.H. Estimation of equivalent thermal parameters of impregnated electrical windings. *IEEE Trans. Ind. Appl.* **2013**, *49*, 2505–2515. [CrossRef]
29. Tang, C.Q.; Yu, Z.J.; Fu, J. Analysis and optimization of a high-speed generator's cooling structure based on Taguchi method. *Case Stud. Therm. Eng.* **2024**, *63*, 105250. [CrossRef]
30. Hebala, A.; Nuzzo, S.; Connor, P.H.; Volpe, G.; Gerada, C.; Galea, M. Analysis and Mitigation of AC Losses in High Performance Propulsion Motors. *Machines* **2022**, *10*, 780. [CrossRef]
31. Preci, E. Experimental Statistical Method Predicting AC Losses on Random Windings and PWM Effect Evaluation. *IEEE Trans. Energy Convers.* **2021**, *36*, 2287–2296. [CrossRef]
32. Mohammed, A.; Djurovic, S. FBG Thermal Sensing Ring Scheme for Stator Winding Condition Monitoring in PMSMs. *IEEE Trans. Transp. Electrif.* **2019**, *5*, 1370–1382. [CrossRef]
33. Duarte, C.A. Radiant heat exchange mediated by gaseous atmosphere. *J. Therm. Anal. Calorim.* **2012**, *107*, 425–430. [CrossRef]

34. Chen, Z.T.; Yu, Z.J.; Fu, J.; Yang, J.T. Analysis and design of air-heat pipe composite cooling of high power density motor. *Appl. Therm. Eng.* **2024**, *236*, 121495. [CrossRef]
35. Liu, H.P.; Ayat, S.; Wrobel, R. Comparative study of thermal properties of electrical windings impregnated with alternative varnish materials. *J. Eng.* **2019**, *17*, 3736–3741. [CrossRef]

Disclaimer/Publisher's Note: The statements, opinions and data contained in all publications are solely those of the individual author(s) and contributor(s) and not of MDPI and/or the editor(s). MDPI and/or the editor(s) disclaim responsibility for any injury to people or property resulting from any ideas, methods, instructions or products referred to in the content.